

NONLINEAR OPTICAL PHENOMENA

PACS numbers: 42.65.Jx; 78.67.–n; 78.67.Sc; 79.20.Ws
DOI: 10.1070/QE2011v041n03ABEH014416

Two-photon absorption and nonlinear refraction of birefringent mesoporous silicon films

V.Ya. Gayvoronsky, L.A. Golovan, M.A. Kopylovsky, Yu.V. Gromov, S.V. Zabotnov, N.A. Piskunov, P.K. Kashkarov, V.Yu. Timoshenko

Abstract. **The self-action of light in birefringent mesoporous silicon films is studied using picosecond laser pulses. Two mechanisms of self-action of light in mesoporous silicon are found. One of them manifests itself at laser intensities below 3 MW cm^{-2} and tends to saturation. The other dominates at intensities above 10 MW cm^{-2}. The former is related to the resonant excitation of electronic states on the surface of silicon nanocrystals, whereas the latter is due to the local fields in the nanocomposite. For the aforementioned ranges of the laser intensity, the cubic nonlinear susceptibility of the films exceeds that of single-crystal silicon by six and four orders of magnitude, respectively, and the figure of merit for the films exceeds that for single-crystal silicon by an order of magnitude.**

Keywords: *two-photon absorption, nonlinear refraction, mesoporous silicon films, picosecond lasers.*

1. Introduction

Semiconductor nanotechnology appears to be promising for new photonics materials. Many semiconductors are known to have quadratic and cubic nonlinear optical (NLO) susceptibilities, which are one-to-two orders of magnitude higher than the corresponding values of the crystals traditionally used in nonlinear optics [1]. Semiconductor-based nanostructures make it possible to increase even more the efficiency of their nonlinear-optical response, which can be used in new photonics devices.

In this paper, we report the results of studying the effects of self-action of light in films of mesoporous silicon (meso-PS). This nanocomposite is formed by silicon nanocrystals from 5 to 100 nm in size (depending on the fabrication conditions), separated by pores of comparable size [2–4].

Previously most attention was paid to microporous silicon (micro-PS), in which the pore size did not exceed several nanometers. This interest was primarily related to the micro-PS photoluminescence in the visible spectral range, which is caused by the quantum-size effect in silicon nanocrystals. The nonlinear-optical properties of micro-PS were actively investigated using the methods of harmonic generation [5–8], photoinduced time-resolved transparency and absorption [9–11], two-photon absorption (TPA) [12, 13], and *z*-scan [14–16]. The results of these studies indicate a decrease in the harmonic generation efficiency for micro-PS in comparison with crystalline silicon (c-Si) [5, 7, 8]. Concerning the real part of the cubic susceptibility $\chi^{(3)}(\omega;\omega,-\omega,\omega)$ (which determines the efficiency of nonlinear refraction), according to [14–16], it ranges from 10^{-12} to 10^{-8} esu. Note that for c-Si $\chi^{(3)}$ it ranges from $(3+0.3\mathrm{i})\times10^{-12}$ [17] to $(7+1\mathrm{i})\times10^{-12}$ esu [18].

The optical properties of semiconductor nanostructures are determined to a great extent by the contributions of the surface electronic states and local-field effects [19]. The formation of pores in the silicon bulk leads to an increase in the surface area and the concentration of surface states per unit volume in this nanocomposite in comparison with the unit volume of c-Si [3]. Local fields are most pronounced in meso-PS; in particular, they cause its birefringence. This effect is due to the preferred orientation of pores in meso-PS in the direction of ⟨100⟩ crystallographic axes [4]. When the substrate is heavily doped c-Si (110), the optical axis of meso-PS coincides with the [001] axis [20].

A simple effective-medium model, which makes it possible to describe well the optical anisotropy of meso-PS, is as follows: silicon nanocrystals and pores are considered as oblate spheroids, whose rotation axes coincide with the [001] crystallographic axis [21]. Then the effective permittivity $\varepsilon_{\mathrm{eff}}$ of meso-PS has anisotropy, and the local field E in silicon nanoparticles is related to the applied field E_0 by a factor $\mathcal{L}_i$: $\boldsymbol{E}_i = \mathcal{L}_i \boldsymbol{E}_{0,i}$. For the electrostatic effective-medium model,

$$\mathcal{L}_i = [1 + L_i(\varepsilon_{\mathrm{Si}} - \varepsilon_{\mathrm{eff},ii})/\varepsilon_{\mathrm{eff},ii}]^{-1}, \quad (1)$$

where $\varepsilon_{\mathrm{Si}}$ is the permittivity of c-Si; L_i is the depolarisation factor, which is determined by the nanocrystal shape and electric field direction; and i is the Cartesian coordinate along one of the spheroid axes. The use of the effective-medium approach for meso-PS is quite justified because the characteristic sizes of nanopores and nanocrystals in this material are smaller than the light wavelength, while meso-PS samples do not exhibit pronounced scattering.

The generalisation of this model to the case of NLO susceptibility of a cubic nanocomposite, which was performed, for example, in [22], yields

V.Ya. Gayvoronsky, M.A. Kopylovsky, Yu.V. Gromov Institute of Physics, National Academy of Sciences of Ukraine, prosp. Nauki 46, 03028 Kiev, Ukraine; e-mail: vlad@iop.kiev.ua;
L.A. Golovan, N.A. Piskunov, V.Yu. Timoshenko Department of Physics, M.V. Lomonosov Moscow State University, Vorob'evy gory, 119991 Moscow, Russia;
S.V. Zabotnov, P.K. Kashkarov Department of Physics, M.V. Lomonosov Moscow State University, Vorob'evy gory, 119991 Moscow, Russia; National Research Centre 'Kurchatov Institute', pl. akad. Kurchatova 1, 123182 Moscow, Russia

Received 3 August 2010; revision received 19 January 2011
Kvantovaya Elektronika **41** (3) 257–261 (2011)
Translated by Yu.P. Sin'kov

$$\chi^{(3)}_{\text{eff},ijkl} = (1-p)\,\mathcal{L}_i(\omega)\chi^{(3)}_{ijkl}(\omega;\omega_1,\omega_2,\omega_3) \times \mathcal{L}_j(\omega_1)\,\mathcal{L}_k(\omega_2)\,\mathcal{L}_l(\omega_3), \quad (2)$$

where p is the porosity.

In accordance with (1) and (2), the optical anisotropy caused by the orientation of pores along appropriate crystallographic directions should manifest itself in the effective cubic susceptibility of meso-PS. Indeed, experiments on the generation of the third optical harmonic in meso-PS demonstrate a significant NLO anisotropy; however, the generation efficiency in meso-PS is an order of magnitude higher than in c-Si [8, 23], which is inconsistent with the aforementioned model. These effects are primarily related to the increase in the local fields in meso-PS. Hence, these fields should be thoroughly studied.

The experimental data on the light self-action, which is rather sensitive both to different electronic states and to the local fields in the nanocomposite [24, 25], supplement well the existing data on the optical properties of meso-PS. The photoinduced changes in the optical absorption coefficient $\Delta\alpha = \beta I$ and the refractive index $\Delta n = n_2 I$, where I is the laser intensity, are characterised by the effective values of the TPA coefficients $\beta \sim \operatorname{Im}\chi^{(3)}_{\text{eff}}$ and nonlinear refraction $n_2 \sim \operatorname{Re}\chi^{(3)}_{\text{eff}}$. Here, we experimentally investigated the self-action of laser pulses in optically anisotropic meso-PS. The experiments were performed on birefringent films, because they allow one to study more thoroughly the manifestation of local-field effects in this material.

2. Measurement results and discussion

Meso-PS films were prepared by electrochemical etching of c-Si (110) wafers with a resistivity of 3 mΩ cm in a HF (48%) : C_2H_5OH = 1 : 1 solution. The etching current densities were 25 mA cm^{-2} (sample A) and 75 mA cm^{-2} (sample B). We used free-standing films, detached from the substrate under a short high-density current pulse. The film thickness (see Table 1), measured with an METAM RV-22 optical microscope, was constant throughout the sample surface. The films obtained were optically anisotropic: their optical axis laid in the surface plane and coincided with the [001] crystallographic direction.

The effective refractive indices of meso-PS films were determined by measuring their transmission spectra in the IR range (0.78–2.0 μm) for ordinary and extraordinary (see Fig. 1) waves on a Bruker IFS 66/v spectrometer. The transmission spectra for the ordinary wave are similar to those shown in Fig. 1; however, the transmittance is 1%–2% lower than that for the extraordinary wave (because of the higher refractive index and reflection coefficient). An analysis of the position of interference maxima and minima [21] allowed us to find the dispersion of the refractive indices for the ordinary and extraordinary waves in samples A and B in the aforementioned spectral region (Fig. 1, inset). The parameters of samples A and B are listed in Table 1.

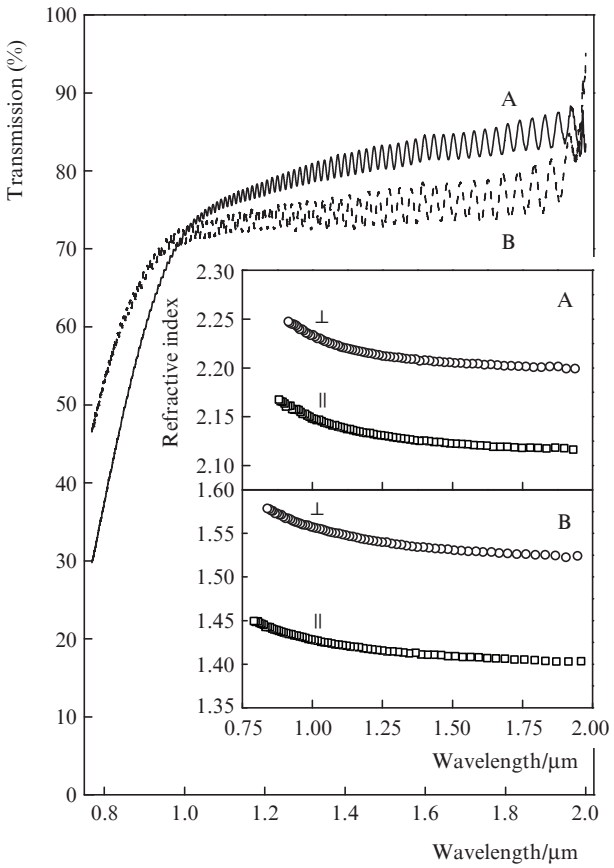

Figure 1. Transmission spectra for an extraordinary wave in mesoporous silicon samples A and B. The inset shows the dispersion relations of the refractive index for (⊥) ordinary and (||) extraordinary waves.

The nonlinear-optical properties of anisotropic meso-PS films were investigated by measuring the distortion of the beam profile in the far field (Fig. 2) [24–29] under self-action of Nd : YAG laser pulses (wavelength, 1.064 μm; pulse width, 42 ps; repetition frequency, 10 Hz). The laser radiation had a Gaussian spatial distribution, and the laser beam was 2 mm in diameter. The laser pulse energy did not exceed 1 mJ, and the radiation intensity on the sample was controlled by a gradient neutral filter. The sample was located behind the plane of the laser beam waist and was oriented so as to make the radiation polarisation direction coincide with either the [1$\bar{1}$0] crystallographic axis (ordinary wave) or the [001] axis (extraordinary wave). During the experiment the radiation intensity was first

Table 1. Structural and optical parameters of the samples and FOM values at a wavelength of 1.064 μm.

Sample	j/mA cm^{-2}	p (%)	d/μm	Polarisation	n	L	$I_0 < 3$ MW cm^{-2}			$I_0 > 10$ MW cm^{-2}		
							$\operatorname{Re}\chi^{(3)}$ (10^{-6})	$\operatorname{Im}\chi^{(3)}$ (10^{-9})	FOM	$\operatorname{Re}\chi^{(3)}$ (10^{-8})	$\operatorname{Im}\chi^{(3)}$ (10^{-13})	FOM
A	25	49	26	⊥	2.22	0.32	4.7	5.9	45	10.8	11.2	56
				||	2.14	0.36	3.0	5.8	29	9.7	6.9	83
B	75	73	24	⊥	1.55	0.30	3.4	1.4	60	2.6	3.4	21
				||	1.42	0.40	2.2	1.5	34	2.7	0.5	143

Note: j is the etching current density; p is the porosity; d is the sample thickness; n is the refractive index; L is the depolarisation factor, and $\chi^{(3)}$ is the cubic NLO susceptibility (in esu).

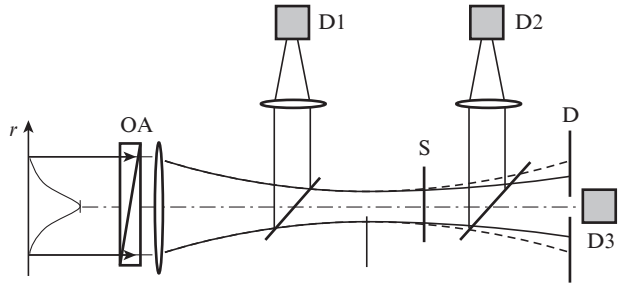

Figure 2. Schematic of the setup: (OA) optical attenuator (gradient filter); (D) diaphragm on the beam axis; (S) sample; and (D1, D2, D3) diodes measuring, respectively, the energy of the incident laser pulse, the total energy of transmitted laser pulse, and the energy of transmitted pulse on the beam axis.

increased and then decreased. All the results demonstrated the reversibility of the response.

The measurements were performed using three photodiodes: diode D1 recorded the laser pulse energy incident on the sample, diode D2 measured the total energy of the beam transmitted through the sample (total sample transmission), and diode D3 measured the laser pulse energy transmitted through the sample at the beam axis (on-axis transmission). To select the contribution of nonlinear refraction against the background of photoinduced absorption, the dependence of the on-axis transmission on the radiation intensity was normalised to the corresponding dependence for the total transmission.

For a plane wave the dependence of the total transmission coefficient T on the intensity I has the form [28]

$$T(I) = T_0/[1 + q(I)], \tag{3}$$

where T_0 is the linear transmission coefficient, $q(I) = \beta I \times [1 - \exp(-\alpha d)]/\alpha$, α is the linear absorption coefficient, and d is the sample thickness. For a Gaussian intensity distribution over radius and a Gaussian pulse temporal shape the dependence of T on the peak intensity I_0 at the beam axis is approximated well by the expression [29]

$$T(I_0) = T_0 \frac{\ln[1 + q(I_0)]}{q(I_0)} \frac{[1 + 0.228q(I_0)]}{[1 + 0.136q(I_0)]}. \tag{4}$$

The radiation transmitted through the sample undergoes absorption, and its phase changes; the transmission coefficient at the light beam axis T_a can be written as a series in the nonlinear phase variation $\varphi_0 = 2\pi n_2 I_0[1 - \exp(-\alpha d)]/(\alpha\lambda)$ (λ is the wavelength) with the coefficients c_i ($i = 1, 2, \ldots$), determined by the geometry of the experiment:

$$T_a(I_0) \approx 1 + c_1\varphi_0 + c_2\varphi_0^2 + \ldots . \tag{5}$$

Having fitted certain ranges of the experimental dependences $T(I_0)$ and $T_a(I_0)$ according to formulas (4) and (5), we find the TPA and nonlinear refraction coefficients [24, 28, 29].

Information about the photoinduced light absorption in meso-PS can be derived from the experimental dependences of the total transmission coefficient T on I_0 (Fig. 3), which contain two characteristic ranges: $I_0 < 3$ MW cm^{-2} and

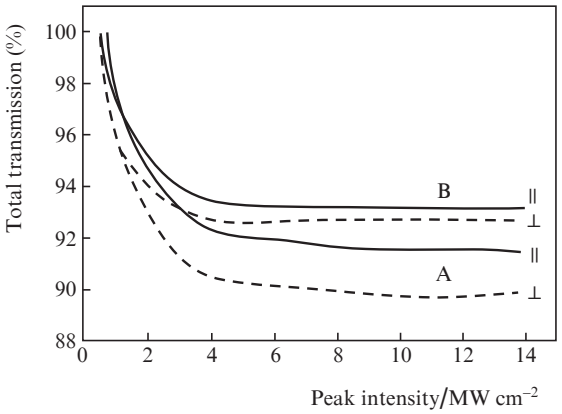

Figure 3. Total transmission of mesoporous silicon films, normalised to their linear transmission, as a function of the peak laser pulse intensity at a wavelength of 1.064 μm for (⊥, dashed curves) ordinary and (||, solid curves) extraordinary waves in samples A and B.

$I_0 > 10$ MW cm^{-2}. The former is characterised by a significant (6%–10%) decrease in the total transmission. Here, the TPA efficiency is practically independent of the polarisation of incident radiation. At large I_0 the decrease in T slows down with an increase in the laser pulse energy and differs significantly for ordinary and extraordinary waves [27].

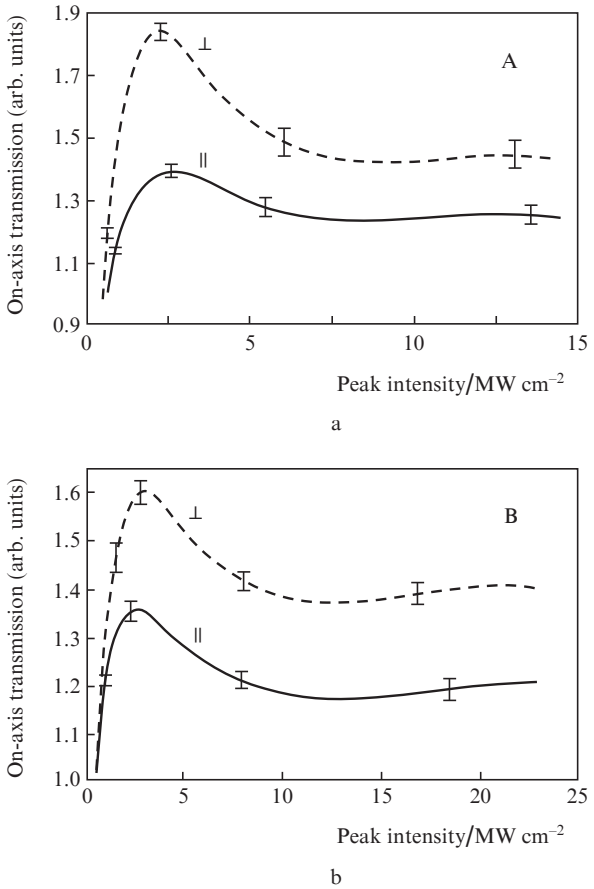

Figure 4. Dependences of the on-axis transmission in the far field, normalised to the total transmission, on the peak laser intensity in the case of (⊥, dashed curves) ordinary and (||, solid curves) extraordinary waves in samples (a) A and (b) B.

In contrast, the dependences of the on-axis transmission coefficients T_a on I_0 (Fig. 4) differ considerably for different polarisations at $I_0 < 3$ MW cm^{-2}: in the case of the ordinary wave the increase in T_a is more pronounced; it is due to the laser radiation self-focusing in the aforementioned intensity range. The $\mathrm{Re}\chi^{(3)}_{\mathrm{eff}}$ value exceeds $\mathrm{Im}\chi^{(3)}_{\mathrm{eff}}$ by three orders of magnitude (Table 1). With a further increase in I_0 the rise in the on-axis transmission first changes to drop (however, its magnitude remains larger than in the linear case), and then (at $I_0 > 10$ MW cm^{-2}) T_a slowly rises.

The used radiation intensity is three orders of magnitude lower than the intensity at which the absorption by free carriers becomes dominant in silicon (40 GW cm^{-2}) [30]; therefore, the contribution of free-carrier generation to the aforementioned effects is insignificant. The difference in the behaviour of the on-axis transmission at low and high laser pulse intensities, as well as its nonmonotonic dependence on the pump radiation intensity, are related to two mechanisms of self-action of light. The former manifests itself at $I_0 < 3$ MW cm^{-2}; in this case both $\mathrm{Re}\chi^{(3)}$ and $\mathrm{Im}\chi^{(3)}$ values in meso-PS are fairly large. This increase in the cubic nonlinear susceptibility can occur when the radiation frequency approaches the transition frequency between some energy states of the material; these states can be related to the defects in the thin silicon oxide layer at the boundaries of nanocrystals and pores. Defects with activation energies of 1.20 and 1.18 eV, which are close to the laser photon energy (1.17 eV), were found at the Si/SiO_2 interface by the photocurrent method [31] and photothermal spectroscopy [32], respectively. The drop in the dependence $T(I_0)$ at $I_0 < 3$ MW cm^{-2} and the weak dependence $T(I_0)$ at $I_0 > 3$ MW cm^{-2}, as well as the nonmonotonic character of $T_a(I_0)$, indicate saturation of the photoinduced effects caused by these states at the peak intensity $I_s \approx 2$–3 MW cm^{-2}. The saturation-induced decrease in TPA is known for a number of semiconductors and organic materials [26, 33, 34]. The drop in the dependence $T_a(I_0)$ at $I_0 > 3$ MW cm^{-2}, which indicates a decrease in n_2, is also typical of the saturation effect [35].

The energy lost in the sample due to the photoinduced absorption is ~10 μJ. Taking into account the sample thickness and laser photon energy, one can estimate the defect concentration per unit volume of the meso-PS layer; it is no less than 10^{16} cm^{-3}. Note that the surface density of these defects was estimated to be 4.7×10^{12} cm^{-2} in [31]; with allowance for the specific surface area of the material (~100 m^2 cm^{-3}), this value yields a volume defect concentration of ~10^{19} cm^{-3} in the meso-PS layer. The difference in the estimated concentrations can be related to the large width of the spectral band corresponding to the aforementioned states (1.15–1.30 eV) [32] and to the fact that only small fraction of defects are involved in the resonant process.

For sample B both $\mathrm{Re}\,\chi^{(3)}$ and $\mathrm{Im}\,\chi^{(3)}$ values are smaller, which is explained by the decrease in the specific surface area of nanocrystals and silicon oxide coating with an increase in the porosity [3]. TPA is almost insensitive to the polarisation of the incident laser radiation, which may be related to its approach to saturation, whereas $\mathrm{Re}\,\chi^{(3)}$ exhibits a significant anisotropy due to the difference in the strengths of the local fields directed along the optical axis and perpendicular to it. Note that the relation $\mathrm{Re}\chi^{(3)}_{\perp\perp\perp\perp}/\mathrm{Re}\chi^{(3)}_{\parallel\parallel\parallel\parallel} = \mathcal{L}^4_\perp/\mathcal{L}^4_\parallel$ [see (2)] is satisfied well for sample A ($\mathrm{Re}\chi^{(3)}_{\perp\perp\perp\perp}/\mathrm{Re}\chi^{(3)}_{\parallel\parallel\parallel\parallel} \approx 1.57$, $\mathcal{L}^4_\perp/\mathcal{L}^4_\parallel \approx 1.5$). For sample B the $\mathrm{Re}\chi^{(3)}_{\perp\perp\perp\perp}/\mathrm{Re}\chi^{(3)}_{\parallel\parallel\parallel\parallel}$ ratio remains nearly the same as for sample A, whereas $\mathcal{L}^4_\perp/\mathcal{L}^4_\parallel \approx 3.4$.

In the range $I_0 > 10$ MW cm^{-2} the $\chi^{(3)}_{\mathrm{eff}}$ values are two orders of magnitude smaller than at $I_0 < 3$ MW cm^{-2}. Nevertheless, in this case the $\mathrm{Re}\chi^{(3)}_{\mathrm{eff}}$ and $\mathrm{Im}\chi^{(3)}_{\mathrm{eff}}$ values are, respectively, three-to-four and one-to-two orders of magnitude larger than the corresponding values for c-Si. The reason is that the NLO response of meso-PS is determined by the contribution of all atoms of silicon nanocrystals, and the anisotropy of $\mathrm{Im}\chi^{(3)}_{\mathrm{eff}}$ is pronounced. The $\mathrm{Im}\chi^{(3)}_{\perp\perp\perp\perp}/\mathrm{Im}\chi^{(3)}_{\parallel\parallel\parallel\parallel}$ ratios are 1.6 and 6.8 for samples A and B, respectively. The ratio for sample A is in agreement with that obtained within the electrostatic effective-medium model (2), whereas for sample B this ratio cannot be described in terms of this approximation. At the same time, the anisotropy of $\mathrm{Re}\chi^{(3)}_{\mathrm{eff}}$ is much smaller than that of $\mathrm{Im}\chi^{(3)}_{\mathrm{eff}}$ (almost zero for the sample with 73% porosity). Along with similar deviations from the model under consideration, which were found in the experiments on third-harmonic generation in meso-PS [8, 23], this circumstance indicates that the electrostatic approximation is not valid in this case, maybe because of the field inhomogeneity in the bulk of meso-PS [8].

The properties of NLO media are often characterised by the figure of merit $\mathrm{FOM} = \Delta n/(\Delta\alpha\lambda) = n_2/(\beta\lambda)$. Our data indicate that for mesoporous silicon at $I > 10$ MW cm^{-2}, depending on the radiation polarisation, the FOM value ranges from 21 (ordinary wave) to 143 (extraordinary wave), whereas for c-Si different estimates yield FOM ranging from 0.17 [17] to 2.9 [18].

3. Conclusions

Two mechanisms of light self-action in optically anisotropic meso-PS have been found for the first time. We relate these mechanisms to the defect states (for radiation intensities below 3 MW cm^{-2}) and to the contribution of local fields in silicon nanoparticles (for radiation intensities above 10 MW cm^{-2}); the former process exhibits saturation. The nonlinear refraction at low intensities and TPA at high intensities have a pronounced anisotropy. It is shown that the figure of merit for meso-PS layers is at least an order of magnitude larger than for c-Si, which indicates good prospects of this material for novel photonics applications.

Acknowledgements. We are grateful to E.A. Konstantinova, A.M. Zheltikov, C.F. Li, and G.Y. Fan for the fruitful discussions. This study was performed using the equipment of the Collective Use Center at M.V. Lomonosov Moscow State University and supported by the National Academy of Sciences of Ukraine (Grant No. 1.4.1 V/141).

References

1. Adair R., Chase L.L., Payne S.A. *Phys. Rev. B*, **39**, 3337 (1989).
2. Cullis A.G., Canham L.T., Calcott P.D.J. *J. Appl. Phys.*, **82**, 909 (1997).
3. Bisi O., Ossicini S., Pavesi L. *Surf. Sci. Rep.*, **38**, 1 (2000).
4. Lehmann V., Stengl R., Luigart A. *Mat. Sci. Eng. B*, **69-70**, 11 (2000).
5. Golovan L.A., Zoteev A.V., Kashkarov P.K., et al. *Pis'ma Zh. Tekh. Fiz.*, **20**, 66 (1994).
6. Kanemitsu Y., Okamoto S., Mito A. *Phys. Rev. B*, **52**, 10752 (1995).
7. Falasconi M., Andreani L.C., Malvezzi A.M., et al. *Surf. Sci.*, **481**, 105 (2001).
8. Golovan L.A., Kuznetsova L.P., Fedotov A.B., et al. *Appl. Phys. B*, **76**, 429 (2003).
9. Dneprovskii V.S., Karavanskii V.A., et al. *Pis'ma Zh. Eksp. Tekh. Fiz.*, **57**, 394 (1993).
10. Klimov V.I., McBranch D., Karavanskii V.A. *Phys. Rev. B*, **52**, R 16989 (1995).

11. Dobryakov A.L., Karavanskii V.A., et al. *Pis'ma Zh. Eksp. Tekh. Fiz.*, **71**, 430 (2000).
12. Malý P., Trojánek F., Valenta J., et al. *J. Lumin.*, **60-61**, 441 (1994).
13. Diener J., Shen Y.R., Kovalev D.I., et al. *Phys. Rev. B*, **58**, 12629 (1998).
14. Henari F.Z., Morgenstern K., Blau W.J., et al. *Appl. Phys. Lett.*, **67**, 323 (1995).
15. Lettieri S., Fiore O., Maddalena P., et al. *Opt. Commun.*, **168**, 383 (1999).
16. Liu H., Fonseca L.F., Weisz S.Z., et al. *J. Lumin.*, **83-84**, 37 (1999).
17. Lin Q., Zhang J., Piredda G., et al. *Appl. Phys. Lett*., **91**, 021111 (2007).
18. Bristow A.D., Rotenberg N., van Driel H.M. *Appl. Phys. Lett.*, **90**, 191104 (2007).
19. Timoshenko V.Yu., Osminkina L.A., et al. *Phys. Rev. B*, **67**, 113405 (2003).
20. Golovan L.A., Timoshenko V.Yu., Kashkarov P.K. *Usp. Fiz. Nauk*, **177**, 619 (2007).
21. Golovan L.A., Konstantinova A.F., et al. *Kristallografiya*, **49**, 174 (2004).
22. Sipe J.E., Boyd R.W., in *Topics Appl. Phys.* Ed. by V.M.Shalaev (Berlin–Heidelberg: Springer, 2002) Vol. 82, p. 1.
23. Zabotnov S.V., Konorov S.O., et al. *Phys. Stat. Sol. (a)*, **202**, 1673 (2005).
24. Gayvoronsky V., Galas A., Shepelyavyy E., et al. *Appl. Phys. B*, **80**, 97 (2005).
25. Gayvoronsky V., Yakunin S., Enikeeva V., et al. *Laser Phys. Lett.*, **3**, 357 (2006).
26. Brodyn M.S., Borshch A.A., Volkov V.I. *Refractive Nonlinearity of Wide-Gap Semiconductors and Applications* (London: Harwood Acad. Publ., 1990).
27. Gayvoronsky V.Ya., Kopylovsky M.A., et al. *Laser Phys. Lett*., **5**, 894 (2008).
28. Sheik-Bahae M., Said A.A., Wei T.-H., et al. *IEEE J. Quantum Electron.*, **26**, 760 (1990).
29. Borshch A.A., Brodyn M.S., Gayvoronsky V.Ya. *Proc. SPIE Int. Soc. Opt. Eng.*, **5024**, 128 (2003).
30. Tien E.-K., Qian F., Yuksek N.S., Boyraz O. *Appl. Phys. Lett.*, **91**, 201115 (2007).
31. Reimann K., Onnasch D. *Z. Physik*, **23**, 239 (1976).
32. Memon A.A., Fukuyama A., Ikari T. *Jpn. J. Appl. Phys.*, **42**, 358 (2003).
33. Rangel-Rojo R., Stranges L., Kar A.K., et al. *Opt. Commun.*, **203**, 385 (2002).
34. Yüksek M., Kürüm U., Gul Yaglioglu H., et al. *J. Appl. Phys.*, **107**, 033115 (2010).
35. McCormick C.F., Solli D.R., Chiao R.Y., et al. *Phys. Rev. A*, **69**, 023804 (2004).